

The Influence of Oxygen on the Nitrogen Content of Autogenous Stainless Steel Arc Welds

A systematic investigation was conducted on the relationship of nitrogen in the weld and oxygen additions to argon and argon-nitrogen shielding gases

BY M. DU TOIT AND P. C. PISTORIUS

ABSTRACT. The influence of an addition of 2% oxygen to argon-rich shielding gas on nitrogen absorption and desorption during the autogenous arc welding of austenitic stainless steels was examined. Six shielding gases, including argon and argon-oxygen, argon-nitrogen, and argon-nitrogen-oxygen mixtures, were used to weld two experimental stainless steels (similar in composition to AISI 310, containing 0.002% and 0.28% nitrogen) and a nitrogen-alloyed stainless steel, previously available under the trade name of Cromanite. The presence of oxygen in the shielding gas was shown to increase the weld metal nitrogen content, stabilize the arc, suppress degassing, and curb porosity. This is attributed to the formation of a molten slag layer at the weld pool periphery during welding. The higher temperatures under the arc suppress the formation of this slag layer in the center of the pool. The slag layer retards nitrogen degassing by reducing the area available for the adsorption of nitrogen atoms prior to recombination. The absorption of monatomic nitrogen from the arc is not strongly affected, since absorption occurs at the interface between the arc plasma and the liquid weld metal, the area not covered by oxide during welding. This results in higher weld metal nitrogen contents.

Introduction

Nitrogen-alloyed austenitic stainless steels offer a unique combination of high strength and excellent toughness (Ref. 1). In addition to its beneficial effect on mechanical properties (Refs. 2–4), nitrogen acts as a strong austenite-forming element in stainless steel (Ref. 5), which favors its

use as a less-expensive substitute for nickel. Nitrogen is also reported to increase resistance to localized corrosion (Refs. 6, 7) and to reduce sensitization effects during welding (Refs. 8, 9).

In nitrogen-alloyed austenitic stainless steels, nitrogen degassing during welding is often a major concern. Nitrogen evolution from the pool increases the risk of porosity and reduces the weld metal nitrogen content, adversely affecting the mechanical properties and corrosion resistance of the joint. The addition of small amounts of nitrogen to the shielding gas has been proposed as a method of curbing nitrogen losses, but this should be done with care to prevent active nitrogen degassing during welding (Ref. 10).

Nitrogen absorption and desorption during arc welding are complex phenomena and no unified theory for the quantitative understanding of the extent of nitrogen dissolution in stainless steel welds has emerged up to this point. This project aims at examining the influence of three variables on nitrogen dissolution during the autogenous arc welding of stainless steel: the shielding gas composition, the base metal nitrogen content, and the weld surface-active element concentration.

During the first phase of this investigation, experimental stainless steels with various nitrogen and sulfur concentrations were welded autogenously in argon and argon-nitrogen shielding gas atmospheres (Ref. 10). The results of this investigation revealed that the weld metal nitrogen content is not influenced to any

significant extent by the base metal nitrogen content in alloys with lower sulfur levels. In alloys with higher sulfur concentrations, however, an increase in base metal nitrogen resulted in higher weld metal nitrogen contents over the entire range of shielding gases evaluated. The nitrogen saturation limit was reached at progressively lower shielding gas nitrogen contents as the base metal nitrogen level increased. Less nitrogen was required in the shielding gas to reach the saturation limit in alloys with higher sulfur concentrations because an appreciable fraction of the base metal nitrogen was prevented from escaping by the higher level of surface coverage.

A kinetic model was developed to describe the effect of shielding gas nitrogen content, base metal nitrogen content, and weld sulfur concentration on nitrogen absorption and desorption during autogenous arc welding (Ref. 11). This model displayed good agreement with experimental results, and revealed that the nitrogen desorption rate constant decreases at higher concentrations of sulfur. This is consistent with a site blockage model, where surface-active elements occupy a fraction of the surface sites required for nitrogen adsorption. The rate constant for the absorption of dissociated nitrogen is not a strong function of the sulfur concentration.

As described above, sulfur was deliberately added to the experimental steels during the first phase of this project to demonstrate the effect of surface-active elements on nitrogen absorption and desorption during welding. Increasing the sulfur content of nitrogen-alloyed stainless steels to reduce nitrogen losses is, however, not feasible in practice, as sulfur increases the likelihood of hot cracking. As an alternative, small amounts of oxygen (another surface-active element) can be added to the shielding gas during welding. Since oxygen is routinely added to shielding gas mixtures for gas metal arc welding of stainless steels to increase arc stability,

KEYWORDS

Autogenous Welding
Nitrogen Absorption
Oxygen Addition
Shielding Gas
Stainless Steel
Sulfur
Weld Pool

M. DU TOIT is Associate Professor, Department of Materials Science and Metallurgical Engineering, University of Pretoria, Pretoria, South Africa. P. C. PISTORIUS is Professor, Department of Materials Science and Metallurgical Engineering, University of Pretoria, Pretoria, South Africa.

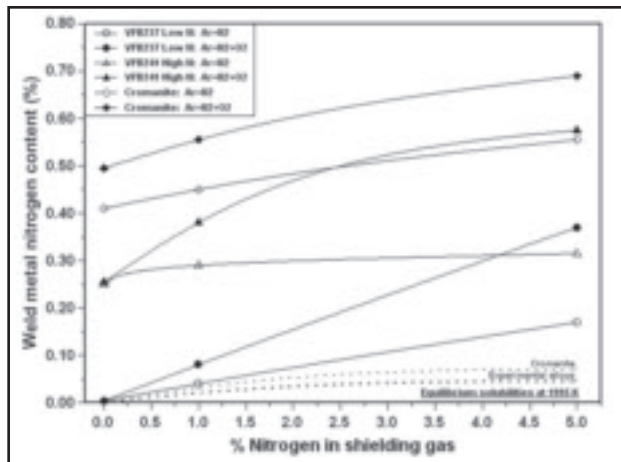


Fig. 1 — The measured weld metal nitrogen content as a function of shielding gas composition. The equilibrium nitrogen levels were calculated as a function of nitrogen partial pressure and alloy composition at a weld pool temperature of 1995 K.

this seems a more viable alternative.

Ample evidence exists to suggest that oxygen influences nitrogen dissolution during welding. Lancaster (Ref. 12) reported that the amount of nitrogen absorbed during arc welding increases in the presence of oxygen, and Ogawa et al. (Ref. 13) demonstrated that nitrogen-induced porosity in austenitic stainless steel welds can be curbed by welding in an oxygen-containing atmosphere. According to Blake (Ref. 14), the presence of oxygen lowers nitrogen desorption rates. Uda and Ohno (Ref. 15) studied the effect of surface-active elements, including sulfur and oxygen, on the nitrogen content of iron during arc melting in Ar-N₂ atmospheres, and reported that surface-active elements increase the nitrogen content and the level of supersaturation in welds. Hooijmans and Den Ouden (Ref. 16) examined nitrogen dissolution in iron containing different amounts of oxygen during arc melting in argon-nitrogen atmospheres. An increase in nitrogen content was observed in samples containing up to 0.008% oxygen. Cross et al. (Ref. 17) reported a significant increase in the nitrogen content of duplex stainless steel welds with as little as 250 ppm oxygen in Ar-N₂ shielding gas mixtures.

Four hypotheses are offered in literature to account for the influence of oxygen on nitrogen dissolution during welding.

1) Blake (Ref. 14) attributed the higher dissolution and lower desorption rates in the presence of oxygen to the formation of NO, resulting from the interaction between nitrogen and oxygen in the arc. The presence of NO in Ar-N₂-O₂ plasmas has since been confirmed by Palmer and DebRoy (Ref. 18) at plasma temperatures below approximately 7000 K, with an associated increase in the amount of

monatomic nitrogen in the arc. Such an increase in the level of monatomic nitrogen in the arc is expected to enhance nitrogen dissolution (Refs. 19–22). The results of emission spectroscopy studies of Ar-N₂-O₂ glow discharge plasmas, however, illustrated that at temperatures higher than approximately 7000 K, NO disappears from the plasma phase, and monatomic species, such as N and O, become dominant (Ref. 18). Calculated and measured temperature profiles within the arc column illustrate that, even in low-current gas tungsten arc welds, temperatures within the arc generally exceed the range where NO is likely to be stable (Ref. 18). This hypothesis also does not account for the higher nitrogen levels observed when welding nitrogen-alloyed stainless steels in oxygen-containing shielding gas without nitrogen. The formation of NO in the welding arc is therefore likely to play a minor role in increasing the nitrogen content of most welds.

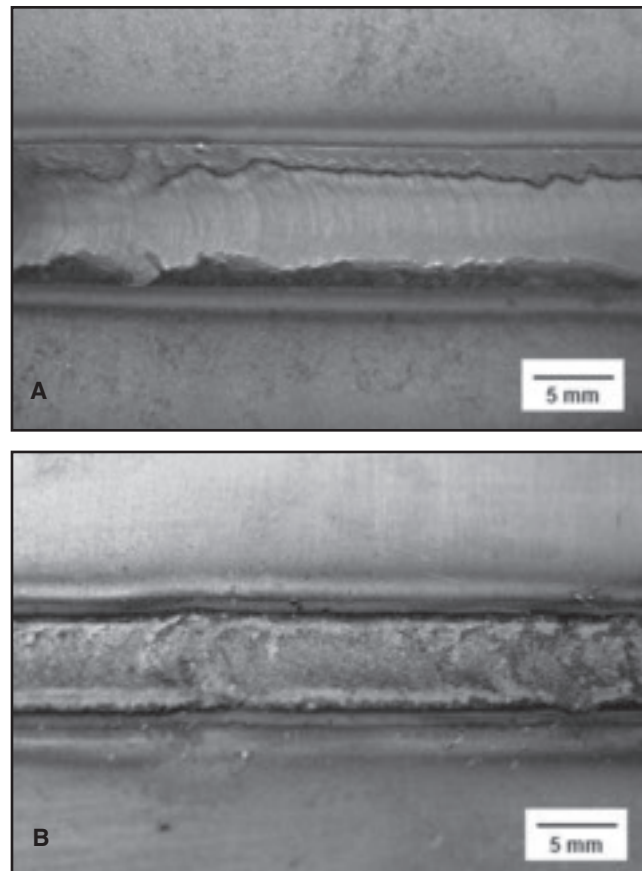


Fig. 2 — The oxide layers observed after autogenous gas tungsten arc welding in argon-rich shielding gas containing 2% oxygen. A — Alloy VFB 241; B — Cromanite.

2) The presence of surface-active elements in the weld pool promotes convergent surface-tension driven (Marangoni) flow. In a pure metal, Marangoni flow is divergent across the weld pool surface, but surface-active elements may cause the gradient of surface tension with temperature to reverse. Surface flow then becomes convergent, causing nitrogen-rich weld metal to flow downward toward the weld root (Ref. 19). In iron-oxygen alloys the gradient of surface tension with temperature reverses at approximately 100 ppm oxygen (Refs. 23–27). Although convergent Marangoni flow in the presence of oxygen probably contributes toward enhanced nitrogen dissolution during low-current gas tungsten arc welding, it is not

Table 1 — Chemical Compositions of the Stainless Steel Alloys Included in this Investigation

Alloy	Comments	Cr	Ni	Mn	Si	C	S	Al	N
VFB 237	Low N	24.7	20.3	2.03	1.52	0.038	0.010	0.0064	0.002
VFB 241	High N	23.8	19.2	2.16	1.81	0.040	0.020	0.0053	0.280
Cromanite™	—	18.1	0.59	9.74	0.29	0.036	0.004	0.0220	0.511

percentage by mass, balance Fe

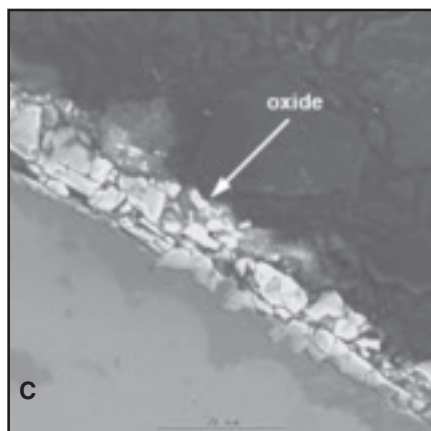
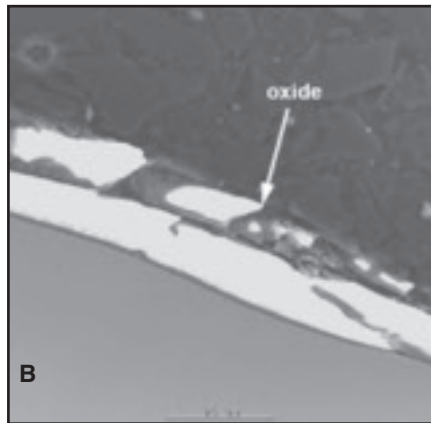
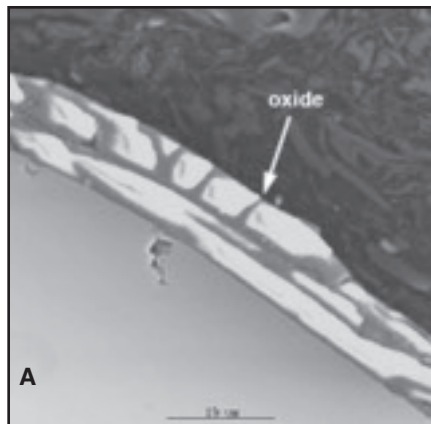


Fig. 3 — Scanning electron micrographs of the surface oxide layers observed on welds performed in shielding gas containing argon and 2% oxygen. A — VFB 237; B — VFB 241; C — Cromanite.

expected to be the dominant mass flow mechanism in most welds.

3) Surface-active elements tend to occupy a fraction of the available surface sites, making it more difficult for nitrogen to adsorb on or desorb from the metal surface (Refs. 19, 28). In view of the results obtained during the earlier stages of this investigation, reduced surface availability may be a viable explanation for the reported influence of oxygen.

4) The formation of an oxide layer on the weld pool surface in the presence of oxygen hampers the outflow of nitrogen

(Ref. 16). Surface oxide formation may be a likely explanation for the effect of oxygen on nitrogen dissolution, and needs to be investigated further.

The objective of this investigation was therefore to systematically examine the influence of oxygen additions to argon and argon-nitrogen shielding gas mixtures on nitrogen absorption and desorption during autogenous arc welding, and to confirm the mechanism responsible for enhanced nitrogen dissolution in the presence of oxygen.

Experimental Procedure

Stainless Steel Alloys

During this investigation, the influence of autogenous arc welding in argon-rich shielding gas containing additions of oxygen and nitrogen on the nitrogen content of two experimental stainless steels was evaluated. The chemical compositions of these alloys, designated VFB 237 and VFB 241, are shown in Table 1. The experimental alloys were designed to have compositions similar to that of AISI 310, an austenitic stainless steel normally produced without deliberate nitrogen addition. This steel was selected as base alloy because it solidifies as austenite and remains fully austenitic down to room temperature. This prevents bulk solid-state phase transformations, which may lead to changes in the solid-state nitrogen solubility, from taking place.

In order to study the influence of the base metal nitrogen content on nitrogen absorption and desorption during welding, the experimental alloys were produced with two nitrogen concentrations: a low nitrogen level (residual nitrogen content of approximately 0.002%), and a high nitrogen level (approximately 0.28%). This nitrogen level exceeds the equilibrium solubility limit of approximately 0.25%, calculated at 1873 K and 1 atmosphere nitrogen pressure.

The third steel included in this investigation is a high-nitrogen austenitic stainless steel that, until recently, was commercially available in South Africa under the trade name of Cromanite™. Whereas nitrogen-alloyed stainless steels are normally produced in pressurized furnaces, where a high-nitrogen partial pressure forces the nitrogen into solution, the high manganese and chromium levels in Cromanite raise the nitrogen solubility to such an extent that it can be produced under atmospheric pressure using conventional steel-making processes. Difficulties encountered during the autogenous arc welding of Cromanite using inert shielding gas (nitrogen losses, porosity, spattering, and metal expulsion from the weld pool) prompted its inclusion in this investigation.

Table 2 — Shielding Gases Used in this Investigation to Examine the Influence of Oxygen and Nitrogen Additions on Nitrogen Dissolution during Welding

Without O ₂ addition	With O ₂ addition
Ar	Ar + 2% O ₂
Ar + 1% N ₂	Ar + 1% N ₂ + 2% O ₂
Ar + 5% N ₂	Ar + 5% N ₂ + 2% O ₂

percentage by volume

Welding Procedure

The stainless steel samples were hot rolled to a thickness of 6 mm, ground and degreased. The plates were welded in a glove box using automatic autogenous gas tungsten arc welding (GTAW). Direct current electrode negative polarity and a 2% thoriated tungsten electrode were used. To minimize atmospheric contamination, the glove box was flushed with argon for at least fifteen minutes prior to welding, and a low argon flow rate was maintained during welding to ensure a slight positive pressure inside the glove box. Shielding was supplied by shielding gas flowing through the welding torch at a rate of 20 L/min. Welding-grade argon and five pre-mixed shielding gases, listed in Table 2, were used. Welding was performed using a current of 150 A, an arc length of 2 mm, and a welding speed of 2.7 mm/s. The measured arc voltage varied from 15.7 ± 0.5 V (95% confidence interval) in shielding gas without oxygen, to 17.3 ± 0.6 V in shielding gas mixtures containing 2% oxygen. Instability of the arc, characterized by flashing, spattering, a hissing sound, and violent metal expulsion from the pool, served as a visual indication of active nitrogen degassing during welding.

It must be emphasized that the addition of oxygen to inert shielding gas during GTAW is not recommended due to oxidation and rapid degradation of the tungsten electrode. Although frequent re-grinding of the electrode was required, the GTAW process was selected for the excellent control it offers over heat input and welding parameters, and because it allows autogenous welding.

After welding, the nitrogen content of each weld was analyzed using an inert gas fusion analysis technique, taking care to remove the metal drillings required only from the weld. At least two analyses were performed on different samples to ensure repeatability. In order to quantify the level of oxygen absorption from the shielding gas, the oxygen contents of welds performed in argon and in an argon-oxygen shielding gas mixture were also measured.

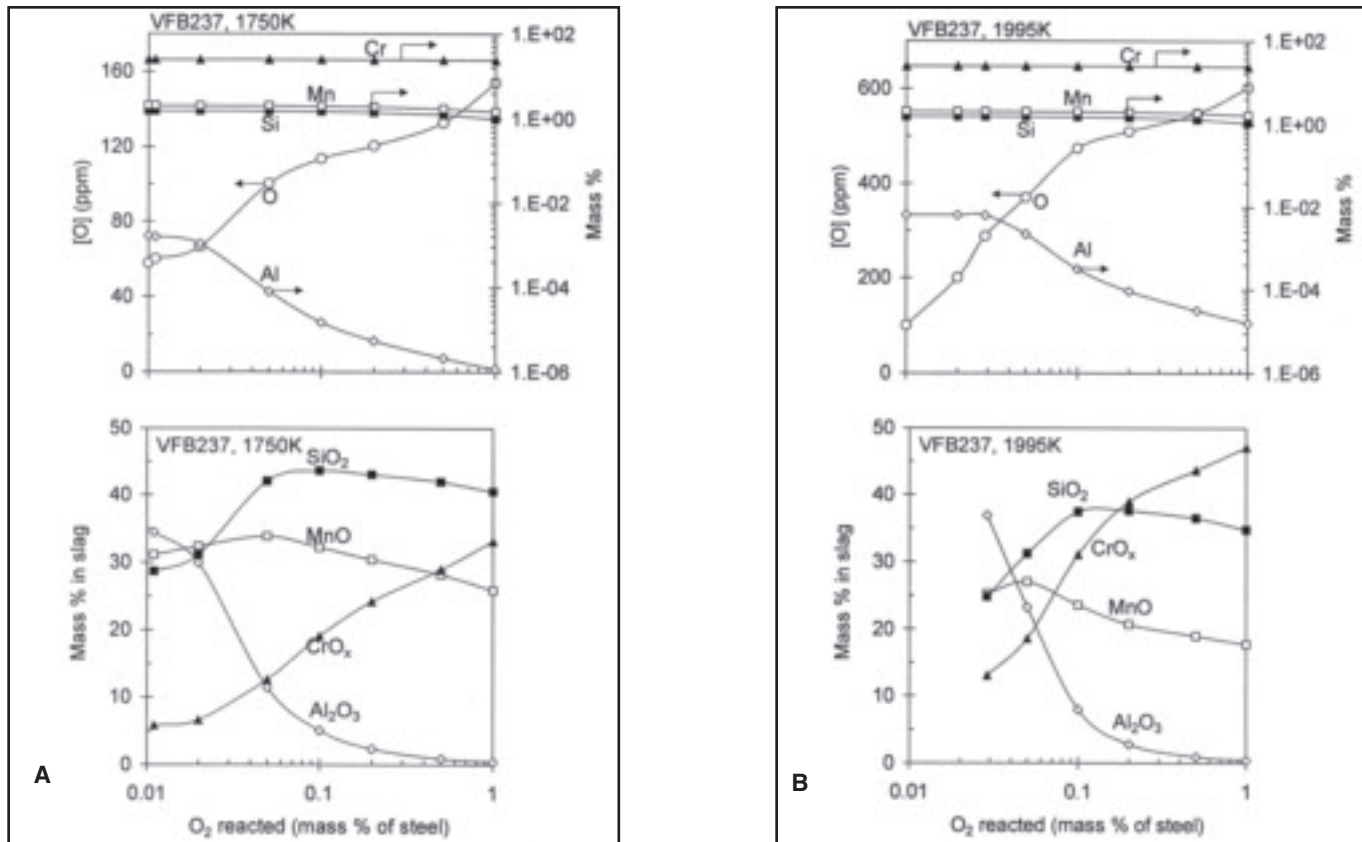


Fig. 4— Calculated equilibrium compositions of the liquid metal (upper graphs) and slag (lower graphs) for VFB 237 weld metal reacted with different amounts of oxygen. The results are shown for two temperatures. A — 1750 K; B — 1995 K.

Results and Discussion

Visual Observation and Weld Metal Nitrogen Content

The average weld metal nitrogen contents are given in Table 3, and shown graphically in Fig. 1. The equilibrium nitrogen solubilities were calculated using Wada and Pehlke's equations and interaction parameters (Ref. 29) at an average weld pool temperature of 1995 K (Ref. 10). Appendix A displays photographs of the welds and details some of the observations made during welding.

Figure 1 confirms that the weld metal nitrogen contents exceed the equilibrium concentrations calculated from Sieverts' law for the shielding gases evaluated. The

addition of nitrogen to the inert shielding gas raises the weld metal nitrogen concentration in all three alloys. The results also demonstrate that the presence of 2% oxygen in the shielding gas increases the weld metal nitrogen contents significantly.

During welding, the experimental steel without any deliberate nitrogen addition (VFB 237) displayed a stable arc in all the shielding gas atmospheres. None of the flashes, spattering, and violent metal expulsion characteristic of active nitrogen degassing was noted, and no porosity was observed on the weld surfaces. The welds were smooth, with fine surface ripples, although more surface oxidation was evident after welding in oxygen-containing shielding gas. Arc stability and the absence of porosity are consistent with the weld

metal nitrogen content remaining below 0.2% in all cases, except for the oxygen-containing shielding gas with the highest nitrogen content (0.2% is the equilibrium solubility limit at 1995 K and 1 atmosphere nitrogen pressure).

The beneficial effect of oxygen was even more apparent on welding the high-nitrogen experimental alloy (VFB 241). Stable arcs were observed when welding in argon and in an argon-oxygen shielding gas mixture. With 1% nitrogen in the shielding gas, the presence of oxygen suppressed nitrogen degassing (even though the measured weld metal nitrogen content exceeds the solubility limit at 1 atmosphere nitrogen pressure) and resulted in a considerably more stable arc. The same trend was observed in shielding gas con-

Table 3 — Average Weld Metal Nitrogen Content of Welded Samples as a Function of Shielding Gas Composition

Alloy	Base Metal N Content	Weld metal N content for various shielding gas compositions					
		Ar	Ar + 2% O ₂	Ar + 1% N ₂	Ar + 1% N ₂ + 2%O ₂	Ar + 5% N ₂	Ar + 5% N ₂ + 2% O ₂
VFB 237	0.002%	0.004%	0.004%	0.040%	0.080%	0.170%	0.370%
VFB 241	0.280%	0.250%	0.255%	0.290%	0.380%	0.315%	0.575%
Cromanite™	0.511%	0.410%	0.495%	0.450%	0.555%	0.555%	0.690%

percentage by mass

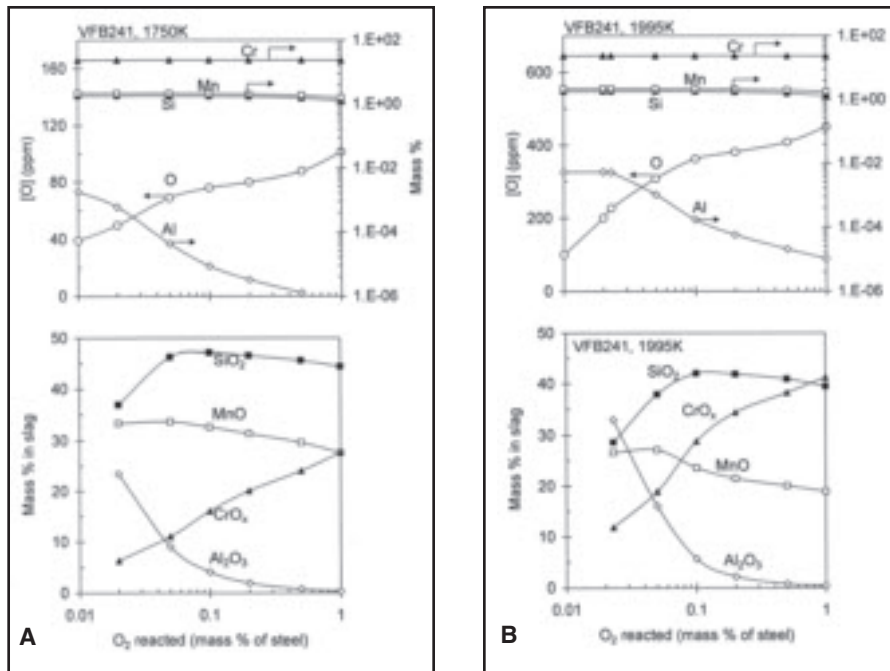


Fig. 5 — Calculated equilibrium compositions of the liquid metal (upper graphs) and slag (lower graphs) for VFB 241 weld metal reacted with different amounts of oxygen. The results are shown for two temperatures. A — 1750 K; B — 1995 K.

taining 5% nitrogen, where the presence of oxygen suppressed nitrogen degassing and reduced porosity. The presence of oxygen in Ar-N₂ shielding gas mixtures resulted in smoother welds, with finer surface ripples.

In Cromanite, welding in argon and argon-nitrogen mixtures caused degassing and porosity. This is consistent with the weld metal nitrogen contents exceeding the equilibrium solubility limit of 0.32% (calculated at 1995 K and 1 atmosphere N₂ pressure) in all cases. The addition of oxygen to the shielding gas resulted in higher

weld metal nitrogen contents in all the shielding gases evaluated. Oxygen also brought about smoother arcs, less degassing, and lower levels of porosity. The addition of 2% oxygen to argon shielding gas eliminated porosity and limited nitrogen losses, resulting in a weld metal nitrogen content comparable to that of the base metal prior to welding (0.495% compared to 0.51% prior to welding, and 0.41% after welding in argon). In nitrogen-containing shielding gas, the addition of oxygen resulted in the formation of fine pores at the weld interface, rather than large pores

within the weld metal. Welds appeared smoother in the presence of oxygen, with finer surface ripples.

Weld Oxygen Content and Surface Availability

The measured weld metal oxygen contents after welding in argon and in argon-oxygen shielding gas mixtures are shown in Table 4. These results indicate that very little oxygen was absorbed by the experimental alloy welds, and that welds produced in argon-oxygen mixtures did not contain significantly more oxygen than welds produced in argon. The beneficial influence of oxygen in suppressing nitrogen degassing is therefore not consistent with a site-blockage model. This was confirmed by estimating the total fraction of vacant surface sites (or the surface availability), (1-θ_T), from Equation 1 (Ref. 19) for each weld. This equation is a simplified version of an equation derived by Byrne and Belton (Ref. 30) to describe the effect of sulfur and oxygen on the fraction of vacant surface sites in the adsorbed surface layer, as determined from measured rate constants for the reaction of N₂ with liquid iron and Fe-C alloys. The slight decrease in surface availability on welding in oxygen-containing shielding gas (amounting to reductions of 3.3 and 8.3% in VFB 237 and VFB 241, respectively) does not adequately explain the observed increase in weld metal nitrogen contents.

$$(1 - \theta_T) = \frac{1}{1 + K_o^{ads} (wt - \%O) + K_s^{ads} (wt - \%S)} \quad (1)$$

where K_O^{ads} is the equilibrium constant for the adsorption of oxygen, given by

Table 4 — Average Weld Metal Oxygen Content after Welding in Ar and Ar-O₂ Shielding Gas Mixtures, and the Calculated Surface Availability at 1995 K

Alloy	Base Metal Oxygen Content	Ar		Ar + 2% O ₂	
		Weld Metal Oxygen Content	Surface Availability	Weld Metal Oxygen Content	Surface Availability
VFB 237	0.030%	0.031%	(1 - θ _T) = 0.361	0.033%	(1 - θ _T) = 0.349
VFB 241	0.020%	0.021%	(1 - θ _T) = 0.411	0.027%	(1 - θ _T) = 0.377
Cromanite™	0.062%	0.022%	(1 - θ _T) = 0.496	0.062%	(1 - θ _T) = 0.297

Table 5 — Weld Pool Depth-to-Width Ratio (D/W) as a Function of Shielding Gas Composition

Alloy	Ar	Ar + 2% O ₂	Ar + 1%N ₂	Ar + 1%N ₂ + 2%O ₂	Ar + 5%N ₂	Ar + 5%N ₂ +2%O ₂
VFB 237	D/W = 0.48	D/W = 0.20	D/W = 0.51	D/W = 0.20	D/W = 0.40	D/W = 0.14
VFB 241	D/W = 0.57	D/W = 0.11	D/W = 0.53	D/W = 0.08	D/W = 0.38	D/W = 0.08
Cromanite™	D/W = 0.32	D/W = 0.28	D/W = 0.43	D/W = 0.24	D/W = 0.34	D/W = 0.24

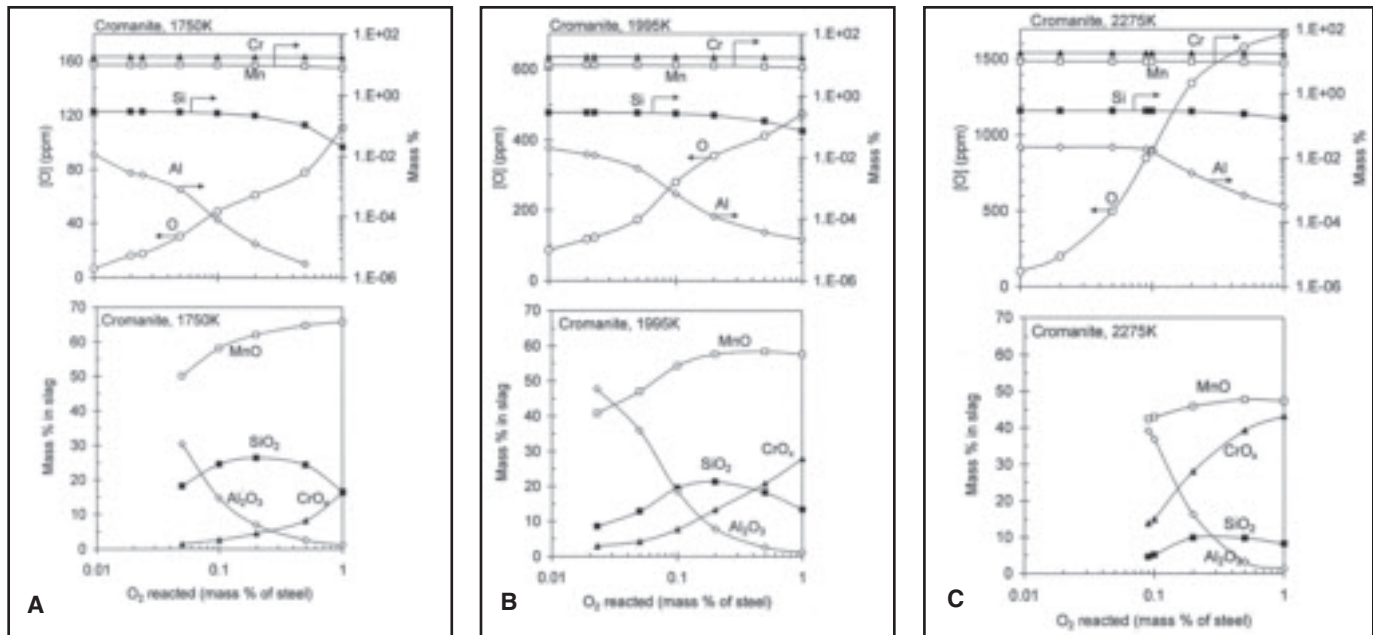


Fig. 6— Calculated equilibrium compositions of the liquid metal (upper graphs) and slag (lower graphs) for Cromanite weld metal reacted with different amounts of oxygen. The results are shown for three temperatures. A — 1750 K; B — 1995; C — 2275 K. For the lowest temperature (1750 K), no liquid slag forms until the amount of reacted oxygen exceeds 250 ppm, as solid Al_2O_3 and $MnAl_2O_4$ form instead. For the two higher temperatures, the absence of slag at lower levels of reacted oxygen indicates that all the oxygen dissolves in the metal.

Equation 2, and K_S^{ads} is the equilibrium constant for the adsorption of sulfur, where K_S^{ads} is assumed to be equal to 65 per wt-% sulfur (reported value at 1873 K).

$$\log K_o^{ads} = \frac{12955}{T} - 4.96 \text{ per wt-\% oxygen} \quad (2)$$

In Cromanite, the weld oxygen content decreased significantly on welding in argon. This may be attributed to effective deoxidation of the weld pool in the presence of high levels of manganese. Welding in an argon-oxygen shielding gas mixture, however, restored the weld oxygen content to its original base metal concentration. This increase in oxygen content, compared to that measured after welding in pure argon, results in a 40% decrease in calculated surface availability. This reduction in surface availability probably played a role in increasing the nitrogen content of Cromanite welds.

Influence of Oxygen on Weld Pool Dimensions

As shown in Table 5, the addition of oxygen to argon-rich shielding gas was observed to change the weld depth-to-width (D/W) ratio. In VFB 237, D/W varied from between 0.40 and 0.51 in shielding gas without O_2 , to 0.2 or less in oxygen-containing shielding gas. The change in weld pool shape was even more pronounced in VFB 241, with D/W varying

Table 6 — Compositions of the Weld Oxide Layers Estimated Using SEM-EDS Analysis

Alloy	SiO ₂	Cr ₂ O ₃	MnO	Al ₂ O ₃
VFB 237	44.2	16.8	38.6	0.4
VFB 241	38.2	19.0	39.3	1.9
Cromanite™	2.3	62.3	26.7	0.9

percentage by mass

from between 0.38 and 0.57 in shielding gas without O_2 , to 0.11 or less in shielding gas containing O_2 . In Cromanite, the addition of oxygen changed D/W from between 0.32 and 0.43 in shielding gas without O_2 , to between 0.24 and 0.28 in shielding gas containing oxygen.

As a surface-active element, oxygen is expected to increase the weld D/W ratio by promoting convergent surface flow in the weld pool. The weld oxygen contents of all three alloys exceed the 100 ppm limit required for convergent flow, ensuring good penetration and high D/W ratios after welding in argon. The addition of oxygen, however, resulted in considerable reductions in the weld D/W ratio in the experimental alloys, even though the weld oxygen levels did not differ appreciably from those measured after welding in argon. This reduction in weld D/W ratio is consistent with results published by Lu et al. (Refs. 23–27). These authors examined the effects of O_2 and CO_2 additions to argon shielding gas on the weld pool shape during GTAW of AISI 304L stainless steel. Their results confirmed that the addition

of up to 0.6% oxygen to argon shielding gas increased the weld oxygen content, resulting in increased weld D/W ratios. With the addition of more than 0.6% oxygen, however, the weld oxygen contents stabilized at levels between 200 and 250 ppm, regardless of the shielding gas oxygen content, and the weld pool shape reverted back to wide, shallow beads with low D/W ratios. This was attributed to the formation of a heavy oxide layer on the weld pool surface in the presence of more than 0.6% oxygen in the shielding gas. This oxide layer apparently inhibits convergent Marangoni flow and acts as a barrier for oxygen absorption. In view of these results, the formation of surface oxides during welding was examined in more detail.

Oxide Formation during Welding

Surface oxide layers were present on all welds performed in oxygen-containing shielding gas. In the experimental alloys, heavy oxide layers were observed at the weld periphery adjacent to the weld interface, while the rest of the weld pool sur-

face remained oxide-free — Fig. 2A. The oxide layers at the weld periphery were continuous, fairly uniform, and tightly adherent. Although a heavy oxide layer was observed at the periphery of Cromanite welds after welding in oxygen-containing shielding gas (Fig. 2B), the oxide layer was not as continuous or adherent as in the case of the experimental alloys, and the oxide appeared to be more granular.

In order to study these surface oxide layers in more detail, cross sections of the welds were mounted in resin, polished to a 3 μm finish, and examined using a scanning electron microscope (SEM). Micrographs of the oxide layers are shown in Fig. 3A – C. The surface oxides on the experimental steels formed continuous layers over short distances at the weld pool periphery, while the central region of the weld was oxide-free. Average oxide thicknesses of $19.7 \pm 3.8 \mu\text{m}$ and $17.1 \pm 4.1 \mu\text{m}$ (95% confidence interval) were measured for VFB 237 and VFB 241, respectively. No oxide particles were observed within the weld metal of the experimental alloys after welding in oxygen-containing shielding gas.

The SEM examination confirmed that the surface layers on Cromanite welds are less uniform, and not as continuous as those observed on the experimental alloys. The average thickness of the Cromanite oxide layer was measured as $17.7 \pm 4.3 \mu\text{m}$. The layer had a granular appearance, and consisted of a mixture of oxide particles and small metal droplets. Although active degassing was not observed during welding in argon-oxygen mixtures, the presence of metal droplets in the surface layer can probably be attributed to nitrogen evolution during welding. It is postulated that the formation of nitrogen bubbles in the weld pool disrupted the oxide layer and generated a spray of metal droplets that became trapped in the oxide layer. Due to the granular nature of the layer, the surface oxide probably acted as a less effective barrier for oxygen absorption, which may account for the higher oxygen content measured in these welds. Small oxide inclusions (5 μm or less in diameter) were observed within the Cromanite weld metal.

The surface oxide compositions were determined using SEM-EDS analysis techniques (Table 6). The oxide layers on the experimental welds were shown to consist of almost equal amounts of SiO_2 and MnO , with some CrO_x (assumed to be Cr_2O_3) and a small amount of Al_2O_3 . No iron was detected in any of the oxide layers. The Cromanite surface oxide layer was shown to consist largely of Cr_2O_3 , with some MnO and low levels of SiO_2 and Al_2O_3 .

Because of the important influence of

the dissolved weld oxygen content on nitrogen absorption and degassing during welding, the factors that control this oxygen content need to be understood. Those elements that form the most stable oxides tend to remove dissolved oxygen from the weld metal. In principle, it is possible to estimate the weld pool oxygen content by calculating the deoxidation equilibria for such elements. This calculation is complicated by the presence of several reactive (deoxidizing) elements in the weld pool, namely aluminum, silicon, manganese, and chromium. The oxide compositions (Table 6) demonstrate that these elements reacted simultaneously, and apparently formed a liquid oxide mixture (slag) on the weld surface.

In order to evaluate the complex reaction equilibrium of the four main reactive elements in the weld pool, the FactSage package (v. 5.4.1) (Ref. 31) was used, with the alloy compositions (Table 1) as inputs. In the calculation, different amounts of oxygen were conceptually allowed to react with the steel to equilibrium. Equilibrium phases considered were the liquid steel (modeled using FactSage liquid solution phase FTmisc-FeLQ (Ref. 32)), liquid slag (modeled using FactSage liquid FToxid-SLAGA), various solid-solution oxides, and stoichiometric oxides such as SiO_2 , Al_2O_3 , MnO , MnAl_2O_4 , and Cr_2O_3 . Two temperatures were used in the majority of calculations. The lower temperature, 1750 K, is approximately 20 K higher than the equilibrium liquidus temperature of AISI 310 and about 40 K higher than the liquidus of Cromanite. This temperature represents the cooler weld pool periphery. The higher temperature, 1995 K, is the average temperature of the pool measured earlier (Ref. 10). An additional temperature, 2275 K, was used in calculating the deoxidation equilibria for Cromanite. This temperature falls within the predicted weld pool peak temperature range, estimated for AISI 304 during GTAW at a current of 150 A and a welding speed of 2.5 mm/s (Ref. 33).

The results of the FactSage calculations are presented in Figs. 4–6. In each of these figures, the metal composition is given in the upper graph, and the composition of the oxide (liquid slag) in the lower graph. If no slag composition is given, no slag formed — typically because all the oxygen dissolved in the metal. In most cases, the oxygen was present in two forms in the equilibrium reaction products: as dissolved oxygen in the steel, and as liquid slag. Occasionally (for the lower reaction temperature), solid Al_2O_3 or (in the case of Cromanite) MnAl_2O_4 were stable, but only at low amounts of reacted oxygen, typically less than 250 ppm. The main form of chromium oxide in the slag was

found to be CrO , with only minor levels of Cr_2O_3 .

For all three steel compositions, Al_2O_3 is a prominent component of the first slag to form. However, the low level of dissolved aluminum is largely removed from the melt at small degrees of reaction with oxygen. The analyzed oxide compositions (Table 6) indicate that, for the experimental steels, the amount of oxygen that had reacted with the weld metal was around 0.1% of the steel mass, yielding a slag consisting mainly of SiO_2 and MnO , with a significant amount of CrO_x . For these intermediate amounts of reacted oxygen, the analyzed weld oxygen content (Table 4) agrees reasonably well with the predicted oxygen content at 1995 K. For this degree of reaction, where the weld contains little aluminum, the dissolved oxygen content is mainly determined by the weld silicon content. This is confirmed by the high slag SiO_2 content, as well as the noticeable difference between VFB 241 and VFB 237: the former has a higher silicon content, which corresponds to a lower dissolved oxygen content. This effect is also noticeable in the weld metal analyses (Table 4).

The situation is rather different for Cromanite (Fig. 6), where MnO is the major slag oxide in most cases. The experimental observations of high weld oxygen contents (Table 4) and high slag CrO_x contents (Table 6) indicate that, for this steel, the analyzed compositions correspond to both a higher equilibration temperature and a higher degree of reaction with oxygen than for the experimental steels.

These calculations confirm that a surface oxide layer forms at the weld periphery on welding in oxygen-containing shielding gas. In all three alloys, more oxygen dissolves in the weld metal at higher temperatures, suppressing the formation of slag at lower amounts of reacted oxygen. The higher temperatures under the arc therefore prevent the formation of a molten slag layer in the central regions of the pool.

Proposed Mechanism

The results of this investigation suggest that the increased weld metal nitrogen contents measured after welding in oxygen-containing shielding gas cannot be attributed only to enhanced convergent Marangoni flow or increased surface coverage. The addition of oxygen to argon shielding gas raised the weld metal nitrogen contents even when mass flow in the pool was clearly divergent. Welding in oxygen-containing shielding gas resulted in higher weld metal nitrogen contents without any significant increase in weld oxygen content, suggesting that reduced surface availability plays a minor role in enhanc-

ing nitrogen dissolution. The conclusion can be drawn that the higher weld metal nitrogen contents observed in the presence of oxygen are mainly due to the formation of a surface oxide layer.

Any mechanism accounting for the role of the surface slag layer has to be consistent with the kinetic model developed earlier (Ref. 11). This model states that the weld metal nitrogen content is determined by the amounts of nitrogen entering and leaving the weld pool per unit time.

Nitrogen enters the pool from the arc atmosphere, i.e., the dissolution of monatomic nitrogen from the arc plasma into the liquid metal, and from nitrogen-containing base metal melting at the leading edge of the pool.

Dissolved nitrogen is removed from the weld pool by recombining to form N_2 molecules that escape to the atmosphere, and through solidification of nitrogen-containing weld metal at the rear of the pool.

Since the travel speed was kept constant, it follows that the melting and solidification rates at the leading and trailing edges of the pool did not vary significantly with changes in shielding gas composition. The presence of a slag layer can therefore influence the amounts of nitrogen entering and leaving the pool due to melting and solidification only through a change in the weld pool dimensions (in particular the pool volume and length). To examine the influence of a change in pool dimensions on the weld metal nitrogen content, the weld pool length and volume were measured after welding in various shielding gases and substituted into the kinetic model. The model revealed that the increase in pool length and volume observed after welding in oxygen-containing shielding gas does not result in any appreciable change in the predicted steady-state weld metal nitrogen content. The presence of a surface slag layer is therefore not expected to affect the amounts of nitrogen entering and leaving the weld pool through melting and resolidification to any significant extent.

The presence of a surface oxide layer can influence the absorption of monatomic nitrogen from the arc and the evolution of nitrogen from the pool by acting as a barrier between the liquid weld metal and the arc atmosphere. Absorption of monatomic nitrogen, however, occurs at the interface between the arc plasma and the liquid weld metal, the area not covered by the oxide layer. Absorption of nitrogen from the arc is therefore not influenced by the presence of oxygen. The recombination of nitrogen to form N_2 molecules occurs over the entire weld pool surface. The presence of a slag layer at the weld periphery is thus expected to retard

nitrogen evolution by reducing the surface area available for the adsorption of atomic nitrogen prior to recombination. The presence of a surface oxide layer at the weld pool periphery therefore reduces the amount of nitrogen leaving the weld pool per unit time, whereas the amount of nitrogen entering the pool is not influenced to any significant extent. This results in an increase in the measured weld metal nitrogen content.

The high nitrogen content measured in Cromanite after welding in oxygen-containing shielding gas can probably be attributed to the high nitrogen solubility in the alloy, the granular nature of the oxide and the higher weld oxygen levels. Since the recombination of adsorbed nitrogen to form N_2 requires two vacant surface sites, and the dissolution of monatomic nitrogen from the arc only one vacant site, the surface slag layer retards nitrogen desorption to a greater extent than nitrogen absorption. The granular nature of the oxide layer therefore facilitates greater nitrogen absorption, while retarding nitrogen desorption in the form of N_2 . This results in high weld metal nitrogen contents after welding in oxygen-containing shielding gas.

Conclusions

- The addition of nitrogen to argon shielding gas during autogenous arc welding raises the nitrogen content of stainless steel welds, but increases the likelihood of active degassing and porosity. An increase in base metal nitrogen content results in higher weld metal nitrogen levels.
- The addition of 2% oxygen to argon and argon-nitrogen shielding gas mixtures increases the weld metal nitrogen content, stabilizes the arc, suppresses degassing and limits nitrogen-induced porosity. The addition of oxygen to the shielding gas does not raise the weld oxygen content to any significant extent.
- Thermodynamic calculation of the deoxidation equilibria in the weld metal demonstrates that a liquid slag layer forms on the weld pool surface during welding in oxygen-containing shielding gas. This slag layer forms readily at the cooler weld periphery, but is suppressed by the higher temperatures under the arc due to increased oxygen solubility in the molten metal.
- The slag layer that forms at the weld periphery in the presence of oxygen retards nitrogen degassing by reducing the surface area available for the adsorption of nitrogen atoms prior to recombination. The absorption of monatomic nitrogen is, however, not strongly affected by the oxide layer, since absorption occurs mostly at the interface between the arc plasma and the liquid metal, the area not covered by oxide

during welding. The surface oxide layer at the weld periphery therefore reduces the amount of nitrogen leaving the weld per unit time, whereas the amount of nitrogen entering the pool is not influenced significantly. This results in an increase in the measured weld metal nitrogen content.

Acknowledgments

Special thanks to Columbus Stainless for performing the nitrogen and oxygen analyses and the University of Pretoria for providing laboratory facilities. The assistance of Karin Frost and Charl Smal is gratefully acknowledged.

References

1. Speidel, M. O., and Uggowitzer, P. J. 1992. High manganese, high nitrogen austenitic stainless steels: their strength and toughness. *Proceedings of the High Manganese, High Nitrogen Austenitic Stainless Steels Conference*, Chicago, Ill., pp. 135–142. ASM International.
2. Reed, R. P. 1989. Nitrogen in austenitic stainless steels. *JOM* 41(3): 16–21.
3. Zackay, V. F., Carlson, J. F., and Jackson, P. L. 1956. High nitrogen austenitic Cr-Mn steels. *Transactions of the American Society for Metals* 48: 509–525.
4. Okagawa, R. K., Dixon, R. D., and Olson, D. L. 1983. The influence of nitrogen from welding on stainless steel weld metal microstructures. *Welding Journal* 62(8): 204-s to 209-s.
5. Franks, R., Binder, W. O., and Thompson, J. 1955. Austenitic chromium-manganese-nickel steels containing nitrogen. *Transactions of the American Society for Metals* 47: 231–266.
6. Janik-Czachor, M., Lunarska, E., and Szklarska-Smialowska, Z. 1975. Effect of nitrogen content in a 18Cr-5Ni-10 Mn stainless steel on the pitting susceptibility in chloride solutions. *Corrosion* 31(11): 394–398.
7. Ogawa, T., Aoki, S., Sakamoto, T., and Zazizen, T. 1982. The weldability of nitrogen-containing austenitic stainless steel: Part I — Chloride pitting corrosion resistance. *Welding Journal* 6(5): 139-s to 148-s.
8. Mozhi, T. A., Clark, W. A. T., Nishimoto, K., Johnson, W. B., and MacDonald, D. D. 1985. The effect of nitrogen on the sensitization of AISI 304 stainless steel. *Corrosion* 41(10): 555–559.
9. Beneke, R., and Sandenbergh, R.F. 1989. The influence of nitrogen and molybdenum on the sensitization properties of low-carbon austenitic stainless steels. *Corrosion Science* 29(5): 543–555.
10. Du Toit, M., and Pistorius, P. C. 2003. Nitrogen control during the autogenous arc welding of stainless steel — Part 1: Experimental observations. *Welding Journal* 82(8): 219-s to 224-s.
11. Du Toit, M., and Pistorius, P. C. 2003. Nitrogen control during the autogenous arc weld-

ing of stainless steel — Part 2: A kinetic model for nitrogen absorption and desorption. *Welding Journal* 82(9): 231-s to 237-s.

12. Lancaster, J. F. 1999. *Metallurgy of Welding*. p. 212, Cambridge, Abington Publishing.

13. Ogawa, T., Suzuki, K., and Zaizen, T. 1984. The weldability of nitrogen-containing austenitic stainless steel: Part II — Porosity, cracking and creep properties. *Welding Journal* 63(7): 213-s to 223-s.

14. Blake, P. D. 1979. Nitrogen in steel weld metals. *Metal Construction* 11(4): 196–197.

15. Uda, M., and Ohno, S. 1973. Effect of surface active elements on nitrogen content of iron under arc melting. *Transactions of the National Research Institute of Metallurgy* 15(1): 20 to 28.

16. Hooijmans, J. W., and Den Ouden, G. 1992. The influence of oxygen on nitrogen absorption during arc melting of iron. *Welding Journal* 71(10): 377-s to 380-s.

17. Cross, C. E., Hoffmeister, H., and Huisman, G. 1997. Nitrogen control in hyperbaric welding of duplex stainless steel. *Welding in the World* 39(3): 154–161.

18. Palmer, T. A., and DebRoy, T. 1998. Enhanced dissolution of nitrogen during gas tungsten arc welding of steels. *Science and Technology of Welding and Joining* 3(4): 190–203.

19. Katz, J. D., and King, T. B. 1989. The kinetics of nitrogen absorption and desorption from a plasma arc by molten iron. *Metallurgical Transactions B* 20B(2): 175–185.

20. Bandopadhyay, A., Banerjee, A., and DebRoy, T. 1992. Nitrogen activity determination in plasmas. *Metallurgical and Materials Transactions B* 23B(2): 207–214.

21. Mundra, K., and DebRoy, T. 1995. A general model for partitioning of gases between a metal and its plasma environment. *Metallurgical and Materials Transactions B* 26B(1): 149–157.

22. Palmer, T. A., and DebRoy, T. 1996. Physical modeling of nitrogen partition between the weld metal and its plasma environment. *Welding Journal* 75(7): 197-s to 207-s.

23. Lu, S., Fujii, H., and Nogi, K. 2004. Marangoni convection and weld shape variations in Ar-O₂ and Ar-CO₂ shielded GTA welding. *Materials Science and Engineering A* 380(1-2): 290–297.

24. Lu, S., Fujii, H., and Nogi, K. 2005. Influence of welding parameters and shielding gas composition on GTA weld shape. *ISIJ International* 45(1): 66–70.

25. Lu, S., Fujii, H., and Nogi, K. 2004. Weld shape comparison with iron oxide flux and Ar-O₂ shielding gas in gas tungsten arc welding. *Science and Technology of Welding and Joining* 9(3): 272 to 276.

26. Lu, S., Fujii, H., Tanaka, M., and Nogi, K. 2004. Effects of welding parameters on the weld shape in Ar-O₂ and Ar-CO₂ shielded GTA welding. IIW Document XII-1801-04, International Institute of Welding.

27. Lu, S., Fujii, H., Sugiyama, H., Tanaka, M., and Nogi, K. 2003. Effects of oxygen addi-

tions to argon shielding gas on GTA weld shape. *ISIJ International* 43(10): 1590–1595.

28. Uda, M., and Ohno, S. 1978. Spattering phenomenon for iron-nitrogen system during arc melting. *Transactions of the National Research Institute of Metallurgy* 20(6): 16–23.













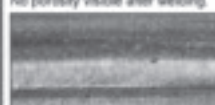




29. Wada, H., and Pehlke, R. D. 1977. Solubility of nitrogen in liquid Fe-Cr-Ni alloys containing manganese and molybdenum. *Metallurgical Transactions B* 8B: 675–682.

30. Byrne, M., and Belton, G. R. 1983. Studies of the interfacial kinetics of the reaction of nitrogen with liquid iron by the 15N-14N isotope exchange reaction. *Metallurgical Transactions B* 14B(3): 441–449.

31. Bale, C. W., Chartrand, P., Degterov, S. A., Eriksson, G., Hack, K., Ben Mahfoud, R., Melançon, J., Pelton, A. D., and Petersen, S. 2002. FactSage thermochemical software and databases. *Calphad* 26(2): 189–228.

32. Jung, I.-H., Decterov, S. A., and Pelton, A. D. 2004. A thermodynamic model for deoxidation equilibria in steel. *Metallurgical and Materials Transactions B* 35B(3): 493–507.

33. Zacharia, S. A., David, J. M., Vitek, J. M., and DebRoy, T. 1989. Weld pool development during GTA and laser beam welding of Type 304 stainless steel. I. Theoretical analysis. *Welding Journal* 68(12): 499-s to 509-s.

APPENDIX A			
Observations made during and after welding. Magnification of the photomicrographs: 1.5x.			
	VFB 237 Low N	VFB 241 High N	Cromaxite
Ar	Stable arc; no flashes, spatter or metal expulsion observed during welding. No porosity visible after welding. 	Stable arc; no flashes, spatter or metal expulsion observed during welding. No porosity visible after welding. 	Unstable arc; spatter, flashes and violent metal expulsion observed during welding. Some porosity visible. 
Ar+2%O ₂	Stable arc; no flashes, spatter or metal expulsion observed during welding. No porosity visible after welding. 	Stable arc; no flashes, spatter or metal expulsion observed during welding. No porosity visible after welding. 	Unstable arc (more stable than in pure Ar); no flashes, spatter or metal expulsion observed. No porosity visible after welding. 
Ar+1%N ₂	Stable arc; no flashes, spatter or metal expulsion observed during welding. No porosity visible after welding. 	Arc somewhat unstable; periodic flashes, metal expulsion and spatter observed during welding. No porosity visible after welding. 	Unstable arc; spatter, flashes and violent metal expulsion observed during welding. Porosity visible after welding. 
Ar+1%N ₂ +2%O ₂	Stable arc; no flashes, spatter or metal expulsion observed during welding. No porosity visible after welding. 	Stable arc; no flashes, spatter or metal expulsion observed during welding. No porosity visible after welding. 	Arc mostly stable; periodic flashes, spatter and metal expulsion. Fine porosity observed adjacent to the fusion line. 
Ar+5%N ₂	Stable arc; no flashes, spatter or metal expulsion observed during welding. No porosity visible after welding. 	Unstable arc; spatter, flashes and violent metal expulsion observed during welding. Porosity visible after welding. 	Unstable arc; spatter, flashes and violent metal expulsion observed during welding. Porosity visible after welding. 
Ar+5%N ₂ +2%O ₂	Stable arc; no flashes, spatter or metal expulsion observed during welding. No porosity visible after welding. 	Arc somewhat unstable; periodic flashes, metal expulsion and spatter observed during welding. Some porosity visible. 	Arc unstable; periodic flashes, spatter and metal expulsion. Fine porosity observed adjacent to the fusion line. 